npj | materials degradation

Article

Published in partnership with CSCP and USTB

https://doi.org/10.1038/s41529-024-00465-7

Short-time high-temperature oxidation behavior of nanocrystalline Ta coating at 850 °C

Yunsong Niu[1,2], Lingling Xing[3], Shenglong Zhu[2] ✉, Jinfeng Huang[1], Minghui Chen[4] ✉, Fuhui Wang[4] & Qiang Chen[5]

Short-time oxidation behavior of nanocrystalline Ta coating is studied at 850 °C in comparison with that of the Ta sheet. Owing to the large PBR value and insufficient expansion space, the oxide scale on Ta sheet is dramatically cracked, delaminated and pulverized, resulting in rapid deterioration. For nanocrystalline Ta coatings with columnar structures and quantitative grain boundaries, a rapid oxygen diffusion rate causes no initial Ta_2O_5 to form. The gap between columns provides spaces for bulk expansion, resulting in few opening cracks and delamination. Ta oxidation experiences a crystallization course from amorphous Ta oxide, leading to in situ temperature surging and thus pulverization.

In weaponry systems, guns and barrels play a significant role by guiding ultrahigh-temperature projectiles through narrow cylindrical tubes with large draw ratios. During firing, substantially, the chemical ammunition substances explode and produce large amounts of gases[1], which results in high temperatures being imposed on the gun bore. Hence, the temperature soars to approximately 1000 °C at the very surface of the gun bore and is maintained for a short period at 700–900 °C[2]. This process will mainly cause chemical conversions, such as oxidation and carbonization after high-temperature gun bore erosion[3]. Lin[4] reported that electrodeposited Cr coating on the inner gun surface could protect against high-temperature erosion and indicated that oxidation can play an important role during the coating failure process, such as CrO_3 evaporation and Cr/CrO_x interfacial mismatch of the coefficient of thermal expansion, leading to a rapid decrease in the thickness of the Cr coating. Furthermore, the effluents from electroplating into natural sinks, soil, and water bodies contaminate and degrade their standards. Although the microelements of chromium have been reported to be significant in living systems, Cr(VI) is beneficial for humans in no way[5].

Tantalum coating deposited by magnetron sputtering, which possesses good ductility, high melting point, high mechanical properties, and excellent chemical inertness at elevated temperatures, is a promising candidate for Cr substitute for gun bore applications[6–9]. However, only a few researchers are concerned about the oxidation of tantalum films. Westwood[10] investigated the effect of low-temperature oxidation on the change in resistance and crystal structure (200–650 °C) of sputtered Ta films before the 1970s. Perkins[11] used acoustic emission technology to detect that oxidation kinetics obey a parabolic law for the initial oxide course at 600 °C and then a linear law after obvious rupture detection by acoustic emission. Chandrasekharan[12] reported that the thermal oxidation behavior of tantalum films obeyed the rules to be logarithmic at 300 °C, followed by parabolic growth at 500 °C and then a multistep growth behavior combined with parabolic and linear growth at 700 °C. The reason for this difference was well discussed by the predecessor: Ta is a highly active refractory metal that can easily absorb oxygen, which turns to form Ta_2O_5 at 260 °C and starts to pulverize above ~600 °C in air[13], leading to poor high-temperature oxidation behavior. Pilling and Bedworth[14] developed a well-accepted concept, the Pilling–Bedworth ratio (PBR), which depicts the volume expansion ratio from a metal to its oxide and describes the structure and protective ability of an oxide layer formed on a metal. A large volume expansion (PBR > 1) is undesirable since it produces increasing compressive stresses inside the oxide with increasing PBR, resulting in cracking or even spalling of the oxide scale. It has been reported that the PBR of pure tantalum is 2.59[15] when orthorhombic β-Ta_2O_5, which is the steady-state thermodynamic equilibrium phase at temperatures below 900 °C, is formed on the substrate. This indicates that β-Ta_2O_5 can consecutively form and delaminate during high-temperature exposure. For tantalum sheets, pulverization can break the integral Ta_2O_5 oxide scale from a metastable state into fragmented powders for approximately several seconds[16,17]. To summarize, as far as we know, no oxidation behavior for short-time oxidation behavior at a high temperature of ~850 °C has been explored, and it is highly difficult to observe the pulverization course and understand its fine mechanism.

[1]State Key Laboratory for Advanced Metals and Materials, University of Science and Technology Beijing, 100083 Beijing, China. [2]Shi-Changxu Innovation Center for Advanced Materials, Institute of Metal Research, Chinese Academy of Sciences, 110016 ShenSyang, China. [3]Shenyang Zhengfa Metal Material Technology Co. LTD, 110143 Shenyang, China. [4]Corrosion and Protection Division, Shenyang National Laboratory for Materials Science, Northeastern University, 110819 Shenyang, China. [5]Southwest Technology and Engineering Research Institute, 400039 Chongqing, China. ✉e-mail: slzhu@imr.ac.cn; mhchen@mail.neu.edu.cn

Therefore, nanocrystalline Ta coating by magnetron sputtering was employed to investigate the oxidation behavior at 850 °C (the temperature range of the gun bore surface immediately after firing) and how to pulverize the material because the intrinsic nanoporous columnar morphology can endure Ta volume propagation; thus, we can determine the details through microstructure observation.

Results

Short-time oxidation behavior of Ta1 sheet

Figure 1 shows the XRD patterns of the surface of the pure Ta sheet after short-time oxidation. With increasing oxidation time, the intensity of substrate peaks decreased gradually, but in contrast, the intensity of the peak attributed to tantalum oxide increased slightly, indicating that the oxide scale quickly increased in thickness and became more complex. Figure 1 clearly shows that two kinds of tantalum oxide appear during oxidation: δ-Ta_2O_5 (PDF# 18-1304, P6/mmm, $\rho = 8.325$ g/cm^3) and β-Ta2O5 (PDF# 25-0922, P21212, $\rho = 9.069$ g/cm^3). δ-Ta_2O_5 was preferentially generated in the initial 30 s. After 60 s, the δ-Ta_2O_5 phase was transformed into β-Ta_2O_5, which dominated the whole tantalum oxide. When Ta sheet is located in the air, it absorbs large amounts of oxygen gas at the surface and into the subsurface due to its extremely high gas-absorbing capacity. Near-to-stoichiometric Ta_2O_5 oxide, a low-temperature steady δ-Ta_2O_5, is the common phase of passivation coating[18]. A rapid temperature shift promoted deep oxygen diffusion and sequential gas-absorbing behavior so that a thick oxide scale formed rapidly in a short 30-s time. Then, the thermodynamic steady-state of the β-Ta_2O_5 phase gradually stabilized after 60 s.

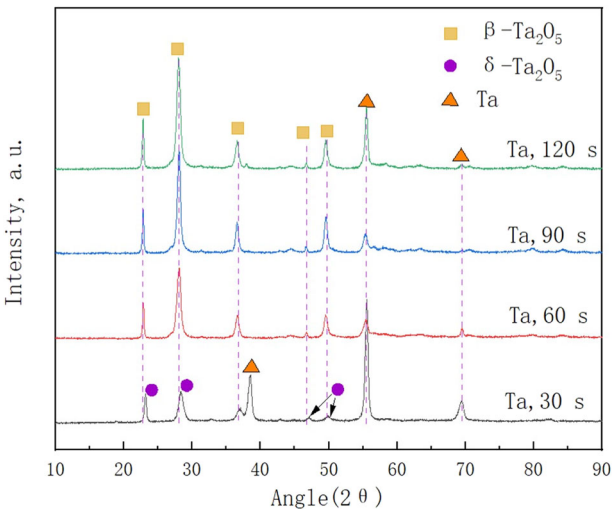

Fig. 1 | XRD patterns of pure tantalum plate after short-time oxidation.

Figure 2 presents the surface morphologies of the Ta sheets after high-temperature oxidation for various durations. Figure 2a shows the surface morphology after 30 s. Partial oxidation occurred, and cracks were produced on the surface of the oxide scale because the PBR value of Ta was 2.47, which is far >1. Therefore, the oxide scale cannot form continuously and protectively, so the bulk expansion from Ta to the δ-Ta_2O_5 phase can lead to quick fracture of the oxide scale. When the oxidation time increased to 60 s, pulverization of the surface oxide scale occurred. After 90 s of oxidation, plenty of pulverized fractures throughout the freshly formed oxide scale caused the Ta substrate to be exposed over a large area. Therefore, the subsurface under the destroyed oxide scale underwent rapid oxidative attack. Repeating in the upper way, a large area of delamination on the Ta surface occurred after 120 s of high-temperature oxidation.

Figure 3 shows the cross-sectional morphologies of the Ta sheets after 30, 60, 90, and 120 s of short-time oxidation. In order to protect the integrity of the oxidation product, an electroless Ni coating was deposited on the corresponding oxidized samples, followed by cutting and preparing a cross-sectional metallographic sample. From the cross-sectional morphology in Fig. 3a, a disordered and non-consecutive oxide scale on the Ta surface formed on the surface with a thickness of 3 μm. At the bottom right corner of Fig. 3a, a magnified photo in Fig. 3a was collected, showing that the melting phenomenon after crystallization occurred in the framed zone. The reason for this will be discussed below. The thickness of the oxide scale increased to

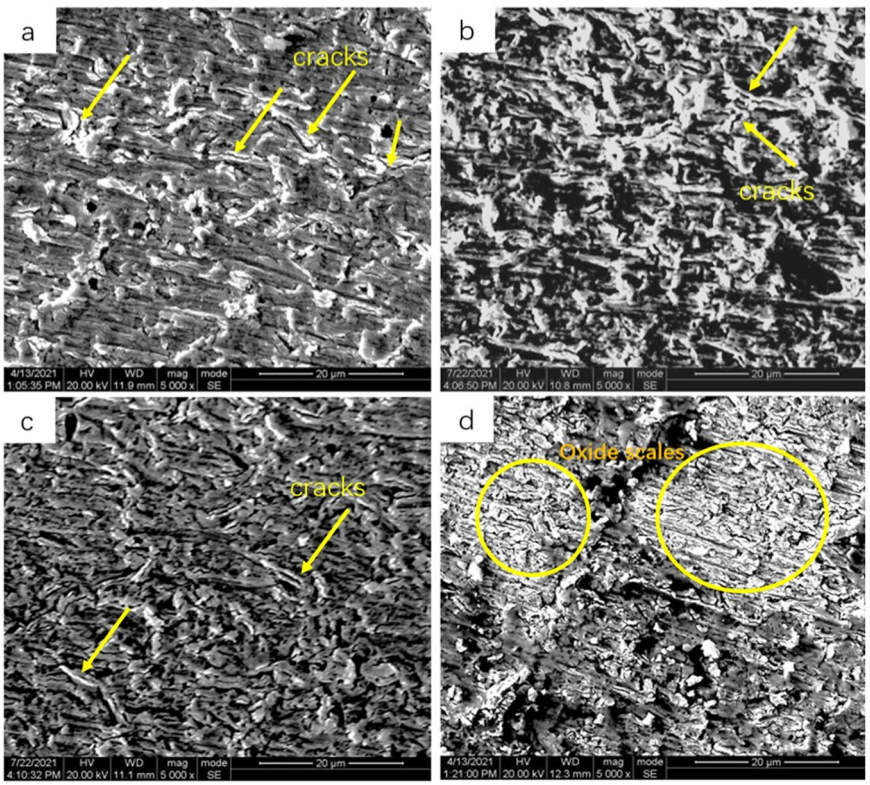

Fig. 2 | Surface morphologies of pure tantalum plate after short-time oxidation. a 30 s; **b** 60 s; **c** 90 s; and **d** 120 s.

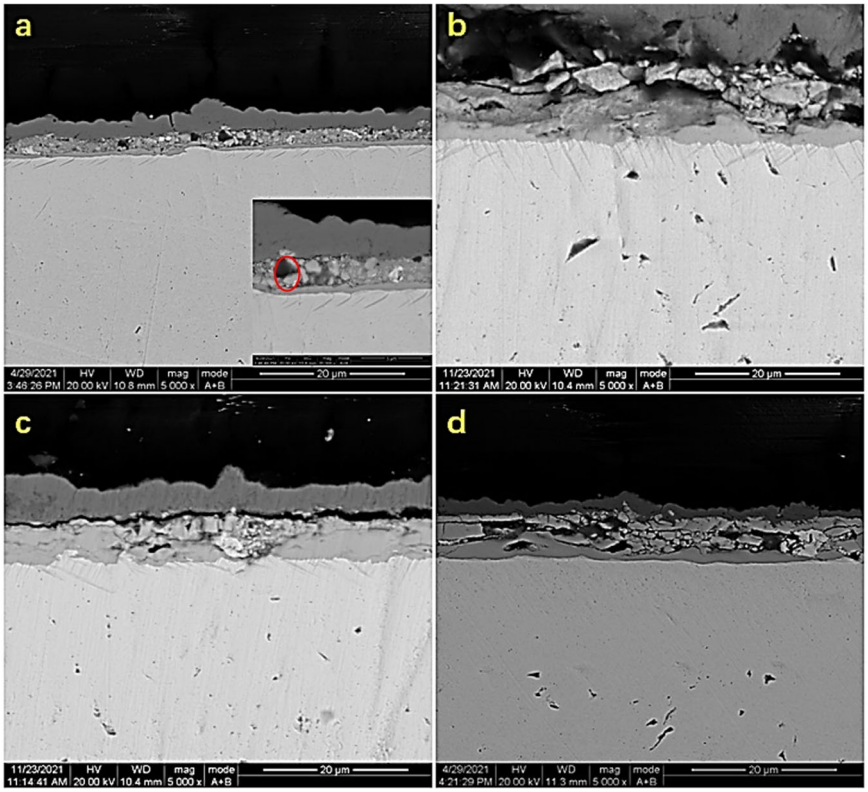

Fig. 3 | Cross-sectional morphologies of pure tantalum plate after short-time oxidation. a 30 s; **b** 60 s; **c** 90 s; and **d** 120 s.

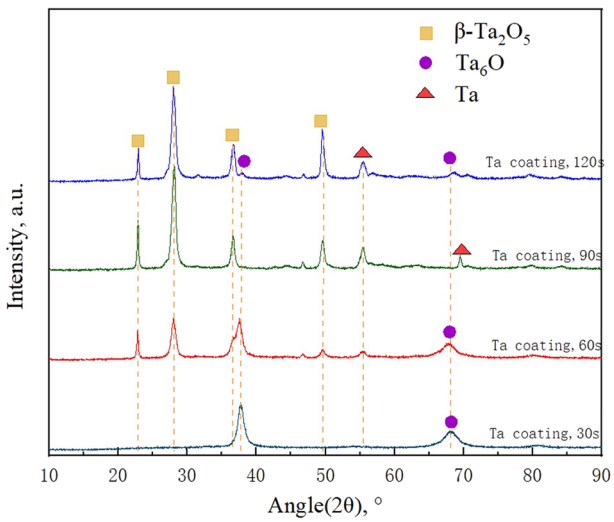

Fig. 4 | XRD patterns of nanocrystalline Ta coating after short-time oxidation.

10 μm, as shown in Fig. 3b, indicating that particles with sizes on the micrometer scale and pulverized and splintered characteristics were about to peel off. Nevertheless, the thickness of the oxide scale decreased suddenly to 7 μm, indicating that the peeling-off behavior happened at least once during the 60–90 s oxidation time, as shown in Fig. 3c, which cannot be captured in detail from the surface morphology. In Fig. 3d, it can be inferred that consecutive pulverization and peeling-off action occurred for a second time due to the large decrease in the thickness of the oxide scale.

Short-time oxidation behavior of nanocrystalline Ta coating

Figure 4 shows the XRD patterns of the nanocrystalline Ta coatings after a short-time oxidation course. From Fig. 4, only a kind of Ta_6O (PDF#15-0206: $a = 3.357$, $c = 3.264$, I4/mmm, $\rho = 16.412$ g/cm^3) suboxide in the low valence state was generated on the Ta coating after a 30 s oxidation time, but no Ta oxide in the full valence state was detected. This is because, in sputtered coatings, the grain size is generally nanosized, thus resulting in quick elemental diffusion of oxygen into deep coatings through large amounts of passages along the crystal boundaries. Together with the high-temperature absorbing and scrambling characteristics, easy, sensitive, and deep diffusion occurred, leading to the formation of unsteady tantalum oxide in the full state but its corresponding suboxide in the low valence state. When oxidation time increased to more than 60 s, the Ta_6O diffraction peak intensity gradually diminished. instead, bcc Ta peaks appeared again. Unlike the Ta sheet, there is no such δ-Ta_2O_5 phase, i.e., a kind of intermediate state emerging during the course of oxidation, and instead, the β-Ta_2O_5 substitution phase becomes dominant and lasts until 120 s of oxidation.

Figure 5 presents the surface morphologies after gradient oxidation time. As shown in Fig. 5a, after 30 s of oxidation, the coating surface is very compact, without any microcracks. According to the calculation from the lattice data, the volume from α-Ta to δ-Ta_2O_5 phase expands to 247% after 30 s of oxidation, while that of the nanocrystalline coatings shrank to ~98.18%, so this shrinkage behavior partially releases the intrinsic internal stress of as-deposited Ta coating. Therefore, the oxidation morphology till 60 s seems unchangingly compact without any microcracks. When oxidation time increased to over 90 s, cracks took place, as shown in Fig. 5c. Only partial delamination of the oxide scale after 120 s happened in Fig. 5d. Therefore, hot internal stress accumulates due to bulk expansion from the α-Ta phase to the β-Ta_2O_5 phase.

Figure 6 shows the cross-sectional morphologies of nanocrystalline Ta coating after gradient short-time oxidation time. As shown in Fig. 6a, a seemingly cracked oxide scale formed on the Ta coating surface due to volume shrinkage behavior. After 60 s of oxidation, the morphology of the oxide scale became very compact. This is the result of phase conversion from the Ta_6O to the β-Ta_2O_5 phase, leading to a volume expansion of ~38.53% in the lattice. This promoted crack healing behavior at a high temperature of 850 °C, resulting in compact oxidation behavior without increasing the

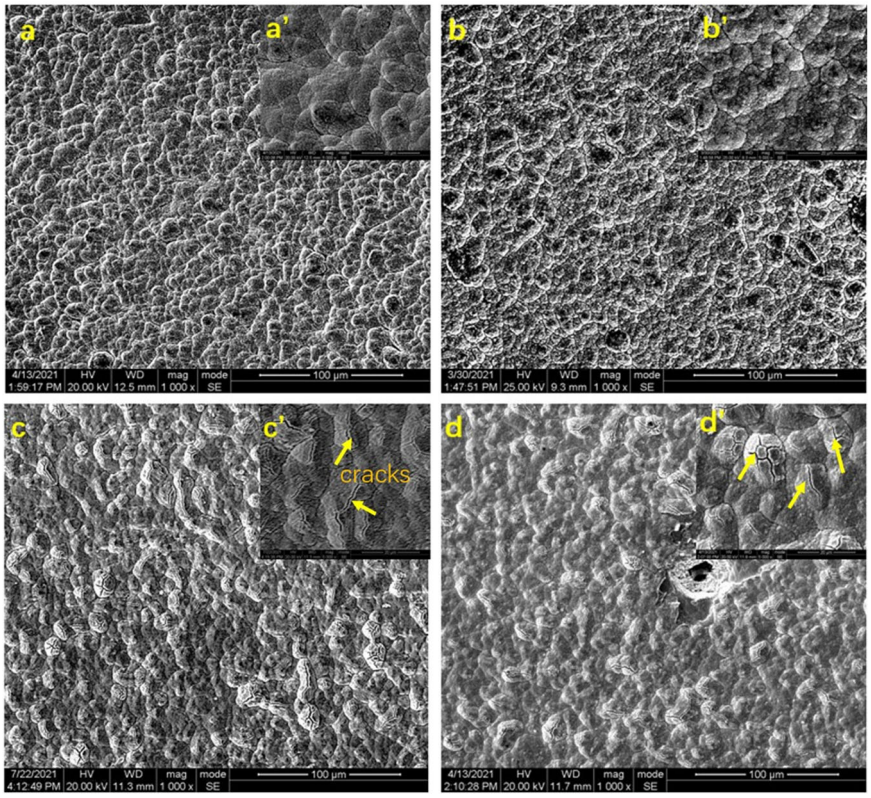

Fig. 5 | Surface morphologies of pure tantalum plate after short-time oxidation. a 30 s; **a**' regional enlargement of (**a**); **b** 60 s; **b**' regional enlargement of (**b**); **c** 90 s; **c**' regional enlargement of (**c**); **d** 120 s; **d**' regional enlargement of (**d**).

oxide scale thickness. This compact coating closed the intrinsic defects of inner passages and pinholes, and then it became a kind of element diffusion barrier in a short time, blocking fast oxygen diffusion. Therefore, according to Figs. 4, 5c, and 6c, only the total β-Ta_2O_5 phase conversion can initiate cracking of the oxide scale. A small amount of inevitable pulverization and delamination occurred with increasing oxidation time, as shown in Fig. 6d.

To further investigate the oxidation mechanism of the nanocrystalline Ta coating, cross-sectional TEM images of the Ta coating after 30 s of oxidation were obtained, and the results are shown in Fig. 7. From Fig. 7a, the morphology for most regions is compact, except for the breakage between the coatings at the top left corner in Fig. 7a, which indicates the volume shrinkage phenomenon of Ta → Ta_6O, which is coincident with Fig. 6a. The SAED results in Fig. 7a mainly show the polycrystalline state of α-Ta, and the appearance of an array of single crystals is the preferred orientation characteristic of the nanocrystalline Ta coating. Figure 7b exhibits the HRTEM morphology of the framed zone in Fig. 7a. Here, apparent Ta oxide layer is only 5 nm thick and is in an approximately amorphous state, as shown in Fig. 7c. From the FFT patterns in Fig. 7d, it can be distinguished of ultrafine-grained Ta_6O and a non-α-Ta diffraction ring, and a detailed analysis is shown in Fig. 8. In other words, the real full-valence-state Ta oxide is only 5 nm in thickness, while the other inner region consists of oxygen-doped tantalum coatings, in coincidence with the XRD results in Fig. 4. The well-adhered and compact Ta oxide with 5 nm seems to have a good effect on protecting the uncracked part beneath it for a period of time.

Figure 8 shows the interface of nanocrystalline tantalum coatings after oxidation for 30 s and corresponding images of the outlined regions processed by the autocorrelation function in several two-dimensional lattice structures, mainly showing the morphology of amorphous tantalum oxide with a completely twisted atomic arrangement. In addition, as shown in Frame 5 of the figure, we also found that the morphology of unoxidized nanocrystalline tantalum still existed in the 5 nm-thick oxide film, but the atomic spacing was slightly greater than that of the α-Ta phase. Furthermore, in the subsurface layer below box a, lattice distortion and an amorphous morphology also appear in boxes g and k, indicating that oxygen has locally diffused from the surface to the matrix and thus cannot form a complete barrier layer. The other boxes represent the bcc atomic arrangement of α-Ta structure. This is also the reason for the appearance of polycrystalline rings in Fig. 7d, indicating that the tantalum oxide scale cannot form a complete and good protective layer. Hence, oxygen is easily enriched at the surface, forming quinquevalent oxides under high oxygen pressure. Meanwhile, quick and convenient oxygen diffusion along the nanograin boundary happens simultaneously toward the inner direction of low oxygen pressure, leading to an incomplete and discontinuous structure of the surface oxide scale. However, quick diffusion did not result in much bulk propagation for the oxide scale, so a comparatively compact structure could be maintained for a period of time rather than generating large-scale crack-like defects.

Figure 9 exhibits the detailed TEM morphologies of inner coating after oxidation for 30 s. Figure 9a–c shows the enlarged morphology and elemental distribution photos in the upper left corner of Fig. 7a, which clearly show the cracks caused by the shrinkage of the tantalum coating and the enrichment of a large amount of oxygen. This fully demonstrates that oxygen will rapidly oxidize here as long as large-scale defects appear in the coating, and the oxidation rate does not bring a gradient downward trend with the increasing crack depth. This is because of the high Ta/O affinity. Moreover, Fig. 9d and e present the enlarged TEM morphology and its corresponding SAED patterns of the framed part in Fig. 9a. This region is mainly composed of amorphous diffraction ring halos, but a large number of diffraction spots of approximately regular crystallization appear on the outer side of the diffraction ring pattern. Furthermore, we conducted HRTEM observation on the frame section, as shown in Fig. 9d, and found that the crystallization of tantalum oxide had already happened locally, resulting in rapid volume expansion. Therefore, the phenomenon of internal oxide collapse in Fig. 9d occurred, which is the reason for the comparatively regular crystallization spots in Fig. 9e.

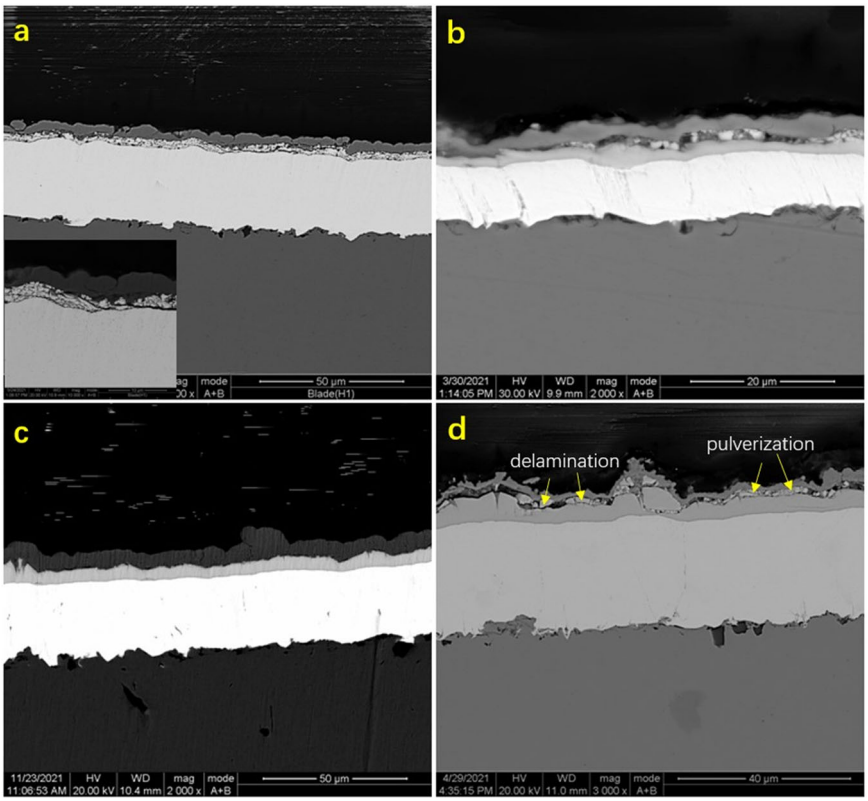

Fig. 6 | Cross-sectional morphologies of nanocrystalline Ta coating after short-time oxidation. **a** 30 s; **b** 60 s; **c** 90 s; and **d** 120 s.

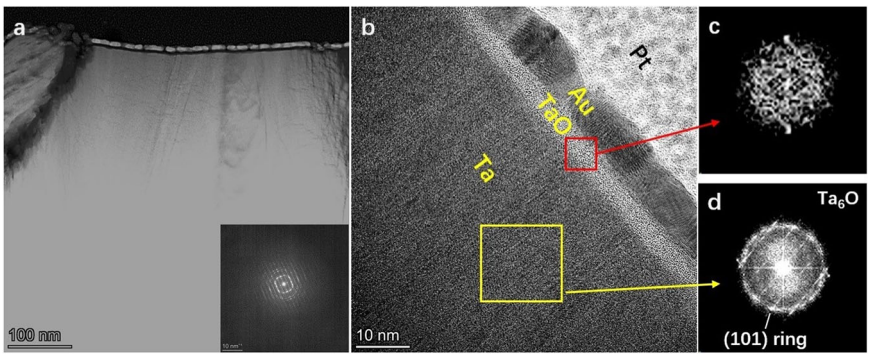

Fig. 7 | TEM observation of nanocrystalline Ta coating after 30 s short-time oxidation. **a** TEM morphology and SAED patterns (**b**) HRTEM image at the very surface in (**a**); **c**, **d** FFT analysis in the framed zones of (**b**).

Discussion

Short-time oxidation mechanism of Ta1 sheet

During the oxidation of tantalum, there are two temperature levels, namely, low-temperature oxidation (300–900 °C) and high-temperature oxidation (>900 °C), and the Ta–O-type oxides generated are also different.

During low-temperature oxidation, the phase of tantalum oxide can include many kinds of L-Ta_2O_5 phases: TaOx, TaOy, TaOz, TaOu, $\alpha_1Ta_{16}O$, $Ta_{12}O$, Ta_6O, $\alpha_1'Ta_4O$, α_2Ta_4O, $\alpha_2'Ta_2O$, TaO, Ta_2O_3, tetragonal δ-TaO_2, hexagonal δ-Ta_2O_5, TT-Ta_2O_5, monoclinic B-Ta_2O_5, triclinic γ-Ta_2O_5, orthorhombic T-Ta_2O_5 and β-Ta_2O_5[19,20]. Among them, $\alpha_1Ta_{16}O$, $Ta_{12}O$, Ta_6O, $\alpha_1'Ta_4O$, α_2Ta_4O, and $\alpha_2'Ta_2O$ are the possible bcc superlattice oxide products for Ta foil at 600 °C for the first step, followed by a vacuum heat treatment at 1500 °C. This means that if diffusion happens, the saturated oxide on the surface can decompose into suboxide with superfine grains. δ-Ta_2O_5 is prone to nucleation and oxidation under the reduction conditions of $Ta^{5+} \rightarrow Ta^{4+}$. Various types of Ta_2O_5 oxides are formed at various temperatures in the air, and the formation laws of different oxide scales have not been well found so far. However, β-Ta_2O_5 is a low-temperature steady-state thermodynamic equilibrium phase[19]. When the temperature exceeds 900 °C, the H-Ta_2O_5 phase consists of only β-Ta_2O_5 and α-Ta_2O_5[21]. When the temperature reaches beyond 1320 °C, the β-Ta_2O_5 phase was converted into α-Ta_2O_5, with an extremely slow transition speed. In this paper, the studied oxidation temperature is 850 °C, which is unconcerned with α-Ta_2O_5.

As for the tantalum plate, its manufacturing process undergoes electron beam melting, rolling, annealing, and removal of surface oxide film[22,23], resulting in the formation of a continuous and dense structure inside the tantalum plate. During the oxidation process, it is difficult to cause rapid inward diffusion of oxygen due to the lack of abundant facilitating passages. Therefore, as a well-known oxygen getter[24–26], the exposure of tantalum in the air at room temperature can result in the intake of abundant oxygen at the surface. When the Ta sheet was placed into a muffle furnace, the surface temperature increased rapidly from room temperature. Then, the chemical bonding between Ta and O from physical absorption occurred above 300 °C[27], i.e., the real oxidation course started. When the surface temperature exceeds 600 °C, an intermediate product of δ-Ta_2O_5 oxide forms quickly due to the already full oxygen-absorbed Ta surface. Ma[28] also reported that δ-Ta_2O_5 oxide has somewhat high-temperature stability in

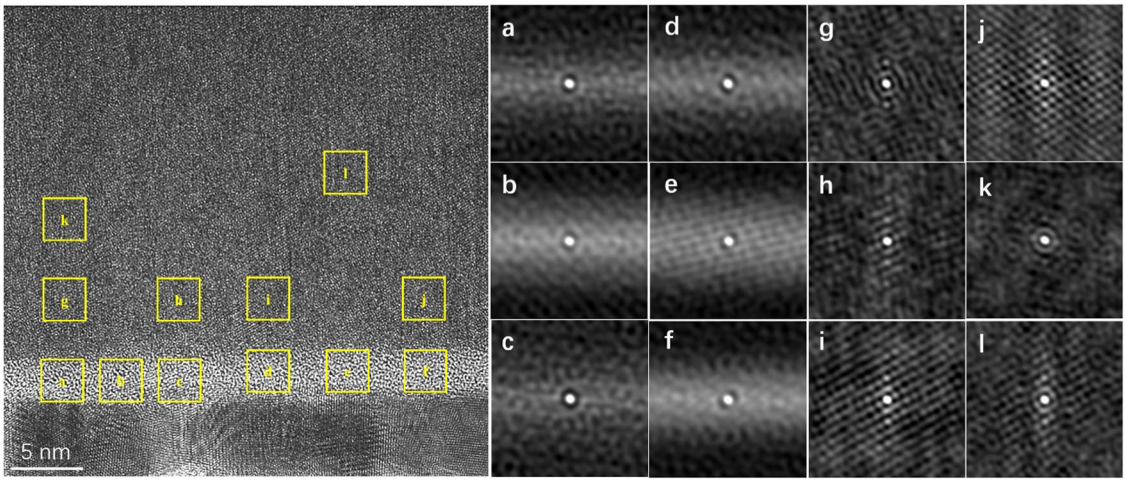

Fig. 8 | Cross-sectional HRTEM image of interface of nanocrystalline tantalum coatings after oxidation for 30 s. a–l corresponding images of the outlined regions processed by the autocorrelation function.

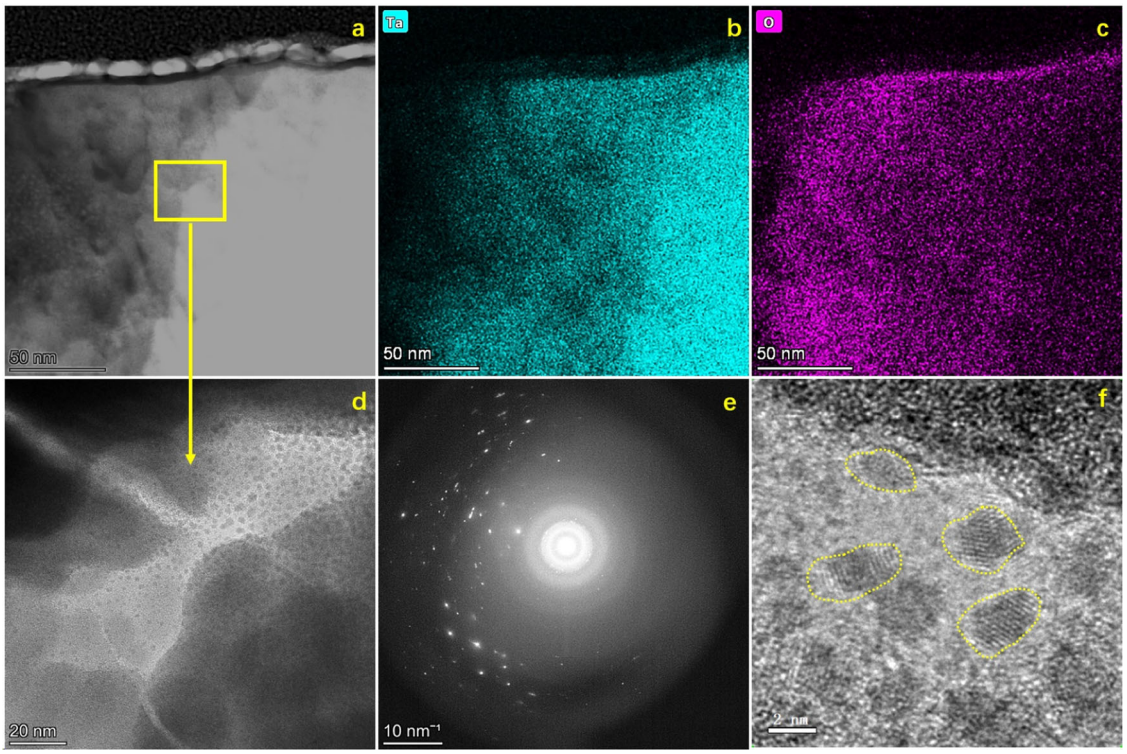

Fig. 9 | Detailed TEM morphologies of inner coating after oxidation for 30 s. a Enlarged TEM morphology from the top left corner in Fig. 7a; **b**, **c** elementary distributions of Ta and O by area scan of TEM; **d** TEM morphology in framed region of (**a**); **e** SAED patterns of (**d**); **f** HRTEM morphology of framed region in (**d**).

comparison with those suboxides and is prone to obtain preferentially. Due to the density difference, the bulk propagation of the Ta → Ta_2O_5 reaction was completed in several seconds, accompanied by propagation and bursting-apart behavior for the outermost surface oxide. Next, the inner Ta substrate was exposed to a high-temperature environment. When the temperature raised between 700 and 1200 °C, the gas absorption performance reached its highest value[29]. Therefore, after less than 30 s, the subsurface layer experienced rapid oxygen absorption and simultaneous oxidation behavior of several micrometers at 850 °C. This is the reason why the surface oxide layer was broken, and the subsurface oxide film seemed dense but did not collapse, as shown in Fig. 3a.

In addition, due to the large PBR value of Ta_2O_5 oxide and its poor matching with the Ta matrix, rapid delamination occurs. As the high-temperature oxidation time prolongs, the tantalum oxides cracked continuously, leading to continuous peeling and further peeling-off of the subsurface layer. This process allows oxidation to rapidly penetrate into the interior of the substrate, resulting in rapid cyclical deterioration of the tantalum blocks.

Short-time oxidation mechanism of nanocrystalline Ta coating

When nanocrystalline Ta coating was oxidized for 30 s, its diffraction peak shifted to the left according to the XRD pattern shown in Fig. 4. We designated the highest peak as the Ta_6O phase by indexing the PDF card and the SAED patterns in Fig. 7a. In the meantime, the broadened peaks also cover the main peaks of α-Ta phase, as proved in Figs. 7 and 8. It is more appropriate to designate this substance as the nonuniform diffusion

interstitial solid solution behavior of tantalum/oxygen[30,31], as the solid solution of oxygen in the bcc Ta lattice increases the internal stress of the nanocrystalline tantalum coating, resulting in the offset of α-Ta phase peaks. Due to the short oxidation time, tantalum oxide crystallization did not occur over a large range, still leading to a generalizing diffraction peak width.

In addition, from the HRTEM analysis, we found that there was no continuous Ta_2O_5 protective layer formed on the surface of tantalum oxide, but a kind of substance, whose atomic spacing is slightly larger than that of the α-Ta phase, is a Ta–O solid solution[32,33]. Garg et al.[19] suggested that the solid solution law of O in Ta between 600 and 1100 °C conforms to Henry's law and can coexist with Ta_2O_5. The following reactions occurred during high-temperature oxidation:

$$\frac{2}{5}Ta + \frac{1}{2}O_2 = Ta_2O_5 \quad (1)$$

$$\frac{1}{2}O_2(g, atm) = O_{in\,Ta} \quad (2)$$

The Gibbs free energy of the products corresponding to reaction Eqs. (1) and (2) can be calculated by the following formula[29]:

$$\Delta_f G^{\theta}_{Ta_2O_5} = -2048.0 + 0.50902T - 0.017439TlnT - 1.4263 \times 10^{-5}T^2 \quad (3)$$

$$G^{\theta}_{O_{in\,Ta}} = 0.2\Delta_f G^{\theta}_{Ta_2O_5} - RTln\,C_s \quad (4)$$

$$ln\,C_s = 1.25 - 1036^{T-1} \quad (5)$$

From formulas (3)–(5), the corresponding values at 850 °C can be calculated: $\Delta_f G^{\theta}_{Ta_2O_5} = -1629.91\ kJ\ mol^{-1}$ and $G^{\theta}_{O_{in\,Ta}} = -3379.06\ kJ\ mol^{-1}$. It can be conducted from the values that the oxygen diffusion and, thus solid solution behavior in tantalum occur highly and simultaneously at 850 °C, which is consistent with the rapid Ta–Ta_2O_5 oxidation reaction occurring on the surface of tantalum. Nanocrystalline coatings can exhibit microscale effects on macroscopic physical and chemical aspects. Due to their nanoscale columnar crystals, there are a large number of grain boundaries and defects in the nanocrystalline coating. The high-density defects in the coating make the interdiffusion of heterogeneous elements easier[34]. Therefore, the presence of high-density grain boundaries provides a convenient channel for the high-speed diffusion of oxygen in tantalum coatings. Due to the extremely low free energy of solid solution diffusion, it preferentially diffuses inwards rather than forming oxide compounds. Therefore, it is difficult for Ta_2O_5 to aggregate on the surface of nanocrystalline tantalum coatings, which is a stark contrast for the oxidation process in comparison to that of rolled tantalum sheets. Due to the heating effect of electron beams, the grain boundary density of pure tantalum plates is low, resulting in a lower diffusion rate of oxygen along their grain boundaries during the oxidation process. The oxidation behavior of tantalum on the surface increases, and tantalum quickly accumulates on the unprotectable Ta_2O_5 scale with pulverizing characteristics, resulting in rapid spalling of the Ta sheet.

According to the oxide layer in Fig. 7b, we can clearly observe that the oxide film on nanocrystalline Ta coating forms a seemingly continuous film with no crack-like opening defects, hindering further inward diffusion of the oxygen medium beyond the transport of anion vacancies. This behavior persists until 120 s, and the cracking phenomenon of the oxide film, which can promote the growth rate of oxide intrusion, only occurs when the thickness of the oxide film reaches about 6 microns (Fig. 6d). This is also attributed to the columnar crystal structure of the nanocrystalline coating (Fig. 2f), which is an inevitable morphology of the coating obtained by physical vapor deposition[35–37]. The spacing between the columnar crystals of the tantalum coating can reach about 20 nm[7], which provides space for the volume expansion generated by the Ta_2O_5 oxidation process, causing the oxide film to gradually densify, resulting in relatively slow oxygen diffusion behavior, as shown in Fig. 6. During the 120 s oxidation process of rolling the tantalum plates, two or more peeling events occurred, and the oxidation depth reached 20 μm.

Pulverizing mechanism during Ta oxidation course

During 30 s of oxidation, the surface of the rolled tantalum sheet has undergone pulverization. This process involves at least five courses, e.g., compound formation, mass accumulation, cracking, delamination, and pulverization. Therefore, it is of great difficulty to seize and observe how and why pulverization is conducted. However, during the initial 30 s of oxidation, nanocrystalline tantalum contracted due to the Ta_6O growth, resulting in longitudinal cracks, as detected in Fig. 7a. At this microscale crack beneath the surface herein, the local oxygen pressure was relatively low compared with the atmospheric conditions for the coating surface. Therefore, we successfully captured the instantaneous pulverization morphology of tantalum oxide, as shown in Fig. 9.

In the early stages of the short-term oxidation process, due to the formation of discontinuous but compact tantalum oxide scale on the surface, which acted as a temporary thermal barrier coating, the temperature rising of the subsurface was relatively slow, and the following reactions occurred below the oxide film:

$$Ta + Ochemsorp \rightarrow Ta - O(solid\ solution) \rightarrow Ta_6O \rightarrow Ta_2O_5 \quad (6)$$

As mentioned earlier, tantalum starts to oxidize at 300 °C, which can result in the formation of amorphous oxides, and when the ambient temperature exceeds 500 °C, the crystallization of amorphous tantalum oxides releases a large amount of heat[38]. In Fig. 9f, it can be seen that some parts of the subsurface layer in the framed zone became crystallized. This region is located inside the crack, which is shown on the left side of Fig. 8a. Here, the crack was not exposed to the air directly but was exposed to low air pressure due to the subsurface site. The upper right direction in Fig. 9f is toward the inner coating, still exhibiting a large area of amorphous state distribution. This not only reflects the thermal barrier effect of Ta_2O_5[39] but also indicates that the crystallization process gradually diffuses from the outside to the inside according to reaction formula 6. Furthermore, the heat generated by crystallization gradually occurs near the surface, inducing the temperature of internal oxidation to rise so that the internal originally amorphous tantalum oxide obtains externally continuous and escalating energies from outside crystallization. With the extension of oxidation time, although the environmental oxidation temperature is only 850 °C, the sharp energy surge from accumulated crystallization heat release causes the local temperature of the subsurface oxide to surpass the melting point of tantalum oxide at a possible temperature peak (Ta_2O_5: 1872 °C, Ta: 2996 °C). This process will bring about the melting and expansion of the tantalum oxide, thus resulting in the outward collapse behavior of the outer oxide scales (Fig. 9d, left side). Moreover, these avalanche particles, possibly joined with other parts of unoxidized tantalum separation from the body coating, become independent individuals attached or disengaged from coatings. Then, they were fully exposed to an atmospheric environment above 850 °C. During the subsequent harsh oxidation process, the density decreases from 16.7 g/cm^3 (α-Ta) to 7.7 g/cm^3 (β-Ta_2O_5) or even lower, and the oxidation process of

Table 1 | Chemical composition of Ta1 tantalum sheet

Element	C	N	H	O	Nb	Fe	Ti	W	Mo	Si	Ta
Content (%)	0.008	0.004	0.0012	0.01	0.04	0.002	0.001	0.005	0.008	0.005	Bal.

external tantalum particles undergoes rapid expansion and continuous collapse behavior as Fig. 9d, resulting in pulverization and disintegration. This is the whole course of how Ta pulverized during high-temperature oxidation.

Short-time oxidation behavior of the nanocrystalline Ta coating, which was obtained by magnetron sputtering technology, was studied for 30, 60, 90 and 120 s at a high temperature of 850 °C and compared with that of the Ta sheet.

For the Ta1 sheet, after only 30 s of oxidation, the δ-Ta_2O_5 phase was generated on the oxide scale of the Ta sheet due to its oxygen-absorbing characteristics with a large bulk expansion ratio. Owing to the PBR value (2.47), the oxide scale on the Ta sheet was dramatically cracked, delaminated and pulverized, without enough expansion spaces for the forged Ta1 metal. Hence, that will result in deep oxidation deterioration into Ta sheet.

For the nanocrystalline Ta coating, a bulk-shrunken Ta_6O phase, a kind of solid-solution strengthened Ta coating by oxygen, was initially formed on the surface. Due to its nanoscale columnar structure and a large number of grain boundaries in the nanocrystalline coating, the diffusion of oxygen by these two defects is very convenient so that no Ta oxide with a full valence state can be produced in the first 30 s of oxidation. Despite the inevitable large bulk expansion behavior from α-Ta to β-Ta_2O_5, the gap between columnar grains provided space for it, resulting in a few opening cracks and delamination phenomena. This compact structure can inhibit quick coating deterioration until 120 s.

Moreover, we developed a low-pressure oxidation method during the initial 30 s of oxidation, and utilizing the bulk shrinkage behavior can yield a momentary crack defect to determine how Ta can pulverize during high-temperature oxidation via TEM observation. During the oxidation course of Ta coating, it will experience a crystallization course from amorphous Ta oxide. This exothermic energy from crystallization accumulates, leading to in situ temperature surging, which can surpass the melting point of tantalum oxide. The avalanche behavior happened together with the surrounding part, becoming independent individuals. The oxidation process of external tantalum particles causes rapid expansion and continuous collapse behavior, resulting in pulverization and disintegration.

Methods

Materials and coating process

304 stainless steel and Ta1 sheet were used as the substrates, which were sandblasted by SiC balls of 220 mesh. An ethanol solution was used to clean the substrate ultrasonically for 10 min before coating deposition. Detailed descriptions of the coating process were reported in our previous work[6]. In order to avoid the diffusional influence of substrate elements during oxidation, the thickness of nanocrystalline Ta coating was ~40 μm. Bare Ta1 sheet (its composition is shown in Table 1) was chosen for analysis of its oxidation mechanism in comparison with that of the N–Ta coating.

Oxidation experiments

High-temperature oxidation test was carried out in a muffle furnace. The temperature was set at 850 °C. The durations of high-temperature oxidation were about 30, 60, 90, and 120 s. Then, the samples were taken out and cooled in air.

Sample characterizations

Electroless nickel plating was utilized to deposit on the samples after oxidation to ensure the integrity of the oxide scales via cross-sectional observation. The cross-sections of the specimens were prepared by cutting, embedding in resin, grinding and then polishing. Phase compositions of the specimens were analyzed by X-ray diffraction (XRD, X'Pert PRO, Cu Kα radiation, 40 kV, 30 mA, 2θ range of 10–90°, step of 0.1°, counting time of 300 s). Microstructure and elemental distributions were determined by scanning electron microscope (SEM, Inspect F50, FEI Co., Hillsboro, OR, USA) and transmission electron microscopy (TEM, FEI Talos F200X), respectively.

Data availability

Data supporting the findings of this study are available from the corresponding author and the first author upon reasonable request.

Code availability

Codes are available upon request to the corresponding authors.

Received: 3 March 2024; Accepted: 10 April 2024;
Published online: 17 May 2024

References

1. Hu, M. et al. Self-ion bombarded Cr films: crystallographic orientation and oxidation behaviour. *Corros. Sci.* **143**, 212–220 (2018).
2. Song, P., Hao, B., Zhang, P., Tang, P. & Zhou, X. Numerical simulation of temperature variation in gun during firing. *Electron. Test.* **4**, 32–35 (2019).
3. Lin, S. S. Auger electron spectroscopic study of gun tube erosion and corrosion. *Appl. Surf. Sci.* **15**, 149–165 (1983).
4. Lin, S. S. Chemical constituents of eroded gun surfaces. *Appl. Surf. Sci.* **21**, 112–124 (1985).
5. Whiteside, J., de Vooys, A. C. A., Sackett, E. & McMurray, H. N. Influence of uniaxial deformation on surface morphology and corrosion performance of chromium-based coatings for packaging steel. *Corros. Sci.* **190**, 109662 (2021).
6. Niu, Y. et al. Phase structure of sputtered Ta coating and its ablation behavior by laser pulse heating (LPH). *J. Mater. Sci. Technol.* **65**, 7–17 (2021).
7. Niu, Y. et al. Preparation and thermal shock performance of thick α-Ta coatings by direct current magnetron sputtering (DCMS). *Surf. Coat. Technol.* **321**, 19–25 (2017).
8. Underwood, J. H., Vigilante, G. N. & Mulligan, C. P. Review of thermomechanical cracking and wear mechanisms in large caliber guns. *Wear* **263**, 1616–1621 (2007).
9. Barnett, B., Trexler, M. & Champagne, V. Cold sprayed refractory metals for chrome reduction in gun barrel liners. *Int. J. Refract. Metals Hard Mater.* **53B**, 139–143 (2015).
10. Westwood, W. D., Waterhouse, N. & Wilcox, P. S. *Tantalum Thin Films* (Academic Press Inc., New York, 1975).
11. Perkins, R. A. & Meier, G. H. Acoustic emission studies of high temperature oxidation. In *High Temperature Materials Chemistry* (eds Munir, Z. A. & Cubicciotti, D.) (Electrochemical Society, New York, 1983).
12. Chandrasekharan, R., Park, I., Masel, R. I. & Shannon, M. A. Thermal oxidation of tantalum films at various oxidation states from 300 to 700 °C. *J. Appl. Phys.* **98**, 114908 (2005).
13. Di, C. Q. et al. Wear behaviors and high-temperature oxidation resistance properties of tantalum carbide layer. *Ceram. Int.* **47**, 32766–32774 (2021).
14. Pilling, N. B. & Bedworth, R. E. The oxidation of metals at high temperature. *J. Inst. Met.* **29**, 529–582 (1923).
15. Hu, K. et al. The effect of surface treatment on the corrosion behavior of pure Ta sheet in an equimolar NaCl–KCl melt at 850 °C in air, part 2: Diamond film, TaC film, Ta–Si coating and Ta–Si–Al coating. *Corros. Sci.* **154**, 11–27 (2019).
16. Kofstad, P. The oxidation behavior of tantalum at 700°–1000 °C. *J. Electrochem. Soc.* **110**, 491–501 (1963).
17. Mazumder, S., Pantawane, M. V. & Dahotre, N. B. Influence of high heating rates on evolution of oxides on directed laser energy additively fabricated IN718. *npj Mater. Degrad.* **5**, 45 (2021).
18. Taratuta, A. et al. Influence of passive layer fabrication method on physicochemical and antimicrobial properties of the Ta_2O_5 layer on NiTi alloy. *Vacuum* **214**, 112187 (2023).
19. Garg, S. P., Krishnamurthy, N. & Awasthi, A. The O–Ta (Oxygen–Tantalum) system. *J. Phase Equilib.* **17**, 63–77 (1996).

20. Yuan, J. H., Xue, K. H., Chen, Q., Fonseca, L. R. C. & Miao, X. S. Ab initio simulation of Ta_2O_5: a high symmetry ground state phase with application to interface calculation. *Ann. Phys.-Berl.* **531**, 1800524 (2019).
21. Tong, Y., Tang, H. & Yang, Y. Structural and electronic properties of Ta_2O_5 with one formula unit. *Comput. Mater. Sci.* **230**, 112482 (2023).
22. Baton, J., Geslin, W. & Moussa, C. Influence of crystallographic orientation on the recrystallization of pure tantalum through microstructure-based estimation of the stored energy. *Int. J. Refract. Met. Hard Mater.* **104**, 105786 (2022).
23. Ma, G., Wei, Z., Wu, G. & Mao, X. The microstructure and strength of a tantalum alloy: influence of temperature. *Mater. Sci. Eng. A* **880**, 145312 (2023).
24. Lafferty, J. M. *Vacuum Technology, Encyclopedia of Physical Science and Technology* 3rd edn (Academic Press, 2003).
25. Nelson, A. T., O'Toole, J. A., Valicenti, R. A. & Maloy, S. A. Fabrication of a tantalum-clad tungsten target for LANSCE. *J. Nucl. Mater.* **431**, 172–184 (2012).
26. Aliyu, A. A. A. et al. Additive manufacturing of tantalum scaffolds: processing, microstructure and process-induced defects. *Int. J. Refract. Met. Hard Mater.* **112**, 106132 (2023).
27. Chandrasekharan, R., Park, I., Masel, R. I. & Shannon, M. A. Thermal oxidation of tantalum films at various oxidation states from 300 to 700 °C. *J. Appl. Phys.* **98**, 114908 (2005).
28. Le, Y., Ma, X., Wang, D., Xiao, H. & Ma, J. Synthesis and characterization of single-crystalline δ-Ta_2O_5 epitaxial films on Y-stabilized ZrO_2 (111) substrates. *Ceram. Int.* **47**, 5510–5514 (2021).
29. Lee, J. S. & Altstetter, C. J. Thermodynamic studies of oxygen behavior in Ta–B based Alloys. *Acta Metall.* **34**, 139–145 (1986).
30. Khachaturyan, A. G. Ordering in substitutional and interstitial solid solutions. *Prog. Mater. Sci.* **22**, 1–150 (1978).
31. Song, C. et al. Study on the influence of oxygen content evolution on the mechanical properties of tantalum powder fabricated by laser powder bed fusion. *Mater. Charact.* **205**, 113235 (2023).
32. Gebhardt, E. & Seghezzi, H. Solubility and oxidation in system Ta–O. *Z. Metallkd.* **48**, 503–508 (1957).
33. Boureau, G. & Gerdanian, E. High temperature thermodynamics of solutions of oxygen in V, Nb and Ta. *J. Phys. Chem. Solids* **42**, 749–753 (1981).
34. Sun, W., Chen, M. & Wang, F. Effect of oxygen doping on the corrosion behavior of nanocrystalline coating under the synergy of solid NaCl deposit and water vapor. *J. Mater. Sci. Technol.* **141**, 257–268 (2023).
35. Senocak, T. C. Characterization and performance of Tantalum–Tungsten based coatings deposited on Cp-Ti substrates by PVD technique. *Mater. Today Commun.* **37**, 107091 (2023).
36. Quillin, K., Yeom, H., Dabney, T., Willing, E. & Sridharan, K. Microstructural and nanomechanical studies of PVD Cr coatings on SiC for LWR fuel cladding applications. *Surf. Coat. Technol.* **441**, 128577 (2022).
37. Cedeño-Vente, M. L. et al. Application of a transmission line model to evaluate the influence of structural defects on the corrosion behavior of arc-PVD CrN coatings. *Ceram. Int.* **47**, 20885–20899 (2021).
38. Kim, N. & Stebbins, J. F. Structure of amorphous tantalum oxide and titania-doped tantala: ^{17}O NMR results for sol–gel and ion-beam-sputtered materials. *Chem. Mater.* **23**, 3460–3465 (2011).
39. Sun, L., Fu, Q. G. & Sun, J. Hot corrosion of SiO_2–Ta_2O_5 binary scale on $MoSi_2$-based ceramics. *Corros. Sci.* **185**, 109413 (2021).

Acknowledgements

The authors gratefully acknowledge the financial support of the project from the National Natural Science Foundation of China (No. 51701223).

Author contributions

Yunsong Niu and Minghui Chen performed the conception and design of the high-temperature oxidation of sputtered Ta coatings. Lingling Xing performed the acquisition, analysis or interpretation of the data. Yunsong Niu, Shenglong Zhu and Jinfeng Huang performed the microscopy of oxidized samples. Fuhui Wang and Qiang Chen supervised this project and the final approval of the completed version. All authors discussed and contributed to the writing of the paper.

Competing interests

The authors declare no competing interests.

Additional information

Correspondence and requests for materials should be addressed to Shenglong Zhu or Minghui Chen.